HHS Public Access

Author manuscript

J Magn Reson Imaging. Author manuscript; available in PMC 2015 August 17.

Published in final edited form as:

J Magn Reson Imaging. 2011 January ; 33(1): 143–148. doi:10.1002/jmri.22418.

Evaluation of respiratory liver and kidney movements for MRI navigator gating

Ruitian Song, PhD, **Aaryani Tipirneni, BS**, **Perry Johnson, MS**, **Ralf B. Loeffler, PhD**, and **Claudia M. Hillenbrand, PhD**

Department of Radiological Sciences, Division of Translational Imaging Research, St. Jude Children's Research Hospital, Memphis, TN 38105-2794, USA

Abstract

Purpose—To determine the tracking factor by studying the relationship between kidney and diaphragm motions and to compare the efficiency of the gating-and-following and gating-only algorithms in reducing motion artifacts in navigator-gated scans.

Materials and Methods—Diaphragm and kidney motions were measured by using real-time TrueFISP sequences from 10 healthy human volunteers in order to determine tracking factors at different acceptance windows. Mean tracking factors were used to calculate mean residual errors and improvement factors for the gating-and-following and gating-only algorithms.

Results—Mean tracking factors for ±4, ±6, ±8 mm and full acceptance windows ranged from 0.6 to 0.7, with large interindividual variations. Acceptance rates increased as the size of the acceptance window increased (acceptance rate for a 4 mm window ~50%). There was a greater reduction of motion errors by gating-and-following (maximum of 1.86 mm) than gating-only (maximum of 7.05 mm).

Conclusions—Mean tracking factors obtained in this study can be used as a guideline for using the gating-and-following algorithm in navigator-gated kidney scans. The gating-and-following and gating-only algorithms were quantitatively compared, and it was found that the former is more effective in reducing motion errors.

Keywords

navigator; kidney/renal imaging; organ movement; kidney tracking; motion correction

INTRODUCTION

MRI of the kidney is widely used in research and clinical practice because of its unique ability to reveal structural and functional status (1). The high spatial resolution and intrinsic tissue contrast offer superb detection and characterization of renal structure. Morphologic MRI of the kidney is used as a routine technique to study the renal parenchyma, and measure renal length and cortical or total kidney volumes. Functional renal imaging

Correspondence to: Claudia M. Hillenbrand, PhD, Department of Radiological Sciences, St. Jude Children's Research Hospital, 262 Danny Thomas Place, Memphis, TN 38105-3678, USA. phone: 901.595.4118, fax: 901.595.3981 claudia.hillenbrand@stjude.org.

techniques [e.g., contrast-enhanced MR to measure glomerular filtration rate (GFR) (2)] and noncontrast methods [e.g., arterial spin labeling (ASL) MRI (3,4), diffusion-weighted imaging (DWI) (5) and blood oxygen level-dependent (BOLD) (6) imaging] have shown promise in evaluating renal function.

A major problem in applying MRI to the kidney is the organ displacement due to respiratory motion. Breath-holding is usually required to minimize respiratory motion, but it relies on good patient cooperation and needs more operator involvement. Even for cooperative patients, misregistration can occur because of the variability between breath-holds. To overcome the problem and improve patients' tolerance, the navigator gating technique was developed to track respiratory motion (7). When navigator gating is used for renal imaging, navigator echoes are used to track the diaphragm position (or the boundary between the lung and liver), and kidney positions are projected on the basis of the tracked diaphragm position: A navigator scan usually is employed before acquiring imaging data.

Navigator gating can be performed by two methods (6): (a) gating-only, in which the kidney is imaged without any position correction when the diaphragm falls within a certain acceptance window, and (b) gating-and-following (also called prospective correction), in which the kidney is imaged with an appropriate tracking factor that is based on the diaphragm position when it falls within the acceptance window. In the gating-and-following approach, the diaphragm position is first measured by a navigator, and then the kidney position is estimated on the basis of the diaphragm position, which is assumed to be correlated with the kidney position by a coefficient called the tracking factor. Because the organ position is corrected, the gating-and-following method is expected to be better than the gating-only method in reducing motion artifacts. This has been qualitatively shown by comparing the quality of coronary MR angiograms obtained with both methods (8). Quantitative analysis will derive more accurate tracking factors that lead to improved image quality.

The effectiveness of suppressing motions highly depends on the accuracy of the tracking factor in the gating-and-following method. The relationship between the movements of the liver and kidney must be examined and an appropriate tracking factor must be determined for the gating-and-following method in navigator gated scans. To the best of our knowledge, there is no systematic evaluation of the relationship between these two movements, although there are some studies on liver and kidney movements focused on radiation therapy planning (9–12). Therefore, in this study, the relationship between the motions in the liver and kidneys was studied by determining the tracking factor, using the True Fast Imaging with Steady-state Precession (True-FISP) (13) sequence. The tracking factor was evaluated and a guideline was given for navigator-gated kidney imaging. In addition, gating-only and gating-and-following methods were quantitatively examined by comparing the residual errors.

MATERIALS AND METHODS

Ten healthy volunteers (20 kidneys, 8 male and 2 female, mean age = 28.1, age range = 21 – 46 year) participated in the study. Written informed consents were obtained from all participants before the exam. Volunteers were scanned on a 1.5T Avanto MRI scanner

(Siemens Medical System, Erlangen, Germany). True-FISP was chosen for the examination because of a high signal-to-noise ratio. The following imaging parameters were used: repetition time (TR) = 3.6 ms, echo time (TE) = 1.8 ms, flip angle = 70°, field of view (FOV) = 32–38 cm, matrix size = 128 × 128, and slice thickness = 7 mm. Participants were positioned supine, with their kidneys at the iso-center of the magnet during image acquisition.

The liver and kidneys were first localized on axial and coronal breath-hold multi-slice scans. After the liver and kidneys were identified, optimal scan planes to examine motions were determined: Coronal and sagittal images crossing the dome of the right hemidiaphragm and kidneys were acquired to examine liver and kidney motions. Scan planes were not angulated. There were 200 consecutive images in each data set, with a time interval of 470 ms, which allowed tracking the motion at 6 or 7 data points per respiratory cycle (respiratory cycle = 3.3 ± 0.5 s). During the scans, volunteers were asked to breathe normally.

To apply the navigator to correct for motion artifacts, the position of the diaphragm was first measured with a 2D excitation beam formed by 90° and 180° slice-selective pulses or a 2D excitation radiofrequency (RF) pulse (7). The imaging position was adjusted prospectively and on the fly on the basis of diaphragm positions measured by the navigator with a scaling factor α, called tracking factor:

$$z_K = \alpha z_L \quad [1]$$

where z_K and z_L are kidney and liver displacement, respectively, along the SI (superior-inferior) axis.

A software program was developed in MATLAB (MathWorks, Natick, MA), with a user-friendly graphical user interface (GUI) to process and examine organ movement. One representative point for each kidney and liver was manually chosen in each image in the dynamic data sets to represent the displacement of the organs of interest. The representative position of the liver was chosen at the top of the liver dome (dome of the right hemidiaphragm), where the navigator ideally is placed. The representative position for the kidneys was the superior pole of each kidney (see Fig. 1). The reference line for each motion was first obtained by averaging the highest points of the motion. The displacement of each point was then measured with respect to the reference line. The displacements for each organ were statistically analyzed by Eq. [1] by using the MATLAB program. The acceptance window was also adapted in the analysis, which was centered at the reference line with different widths.

If the diaphragm position was within the acceptance window, the acquired data was accepted. Otherwise, the data was rejected. The acceptance rate r, defined as the ratio of the number of accepted navigator scans to the total number of navigator scans, was calculated for different acceptance windows for all volunteers. To evaluate the efficiency of the gating-and-following algorithm, residual error, δ measured in mm, was introduced as the mean absolute difference between the real and projected (i.e. calculated via Eq. [1] from the liver position) kidney positions. The effectiveness of the gating-and-following algorithm was

examined by using a mean tracking factor for each volunteer. Mean residual errors were calculated for both the gating-and-following (δ) and gating-only (δ_0) methods for different acceptance windows by using the MATLAB program. The residual error reflects the effectiveness of motion suppression when navigators are used. The residual value should be zero if the motion is ideally compensated. In order to achieve a satisfactory degree of motion suppression, the value of the residual error has to be much lower than the slice thickness for an axial scan or the pixel size for coronal or sagittal scans. The obtained data were statistically analyzed using a MATLAB program.

RESULTS

Figure 2 shows the displacements of the liver and kidneys along with the projected motion of the kidney for a healthy volunteer (volunteer 10). The movement patterns of the two organs were well correlated, because both were induced by respiration. The projected motion is a good approximation of true kidney motion as shown in the figure. The amplitude of motion of the liver was larger than that of the kidney.

Motion of the liver correlated with that of the kidney significantly (linear correlation coefficient R^2 = 0.84–0.98 by statistical analysis). Table 1 summarizes the mean maximal displacements for the liver and the left and right kidney for the 10 volunteers. There was a wide variation in maximum displacements for the liver (7.8–22.5 mm) and kidneys (4.4–15.1 mm). The height and weight information is also listed in the table. No significant correlations were found between the displacements and heights or weights of the volunteers in this study ($R^2 < 0.01$ for displacements vs. heights or weights).

Table 2 gives the acceptance rates (r) and tracking factors (a) for ±4 mm, ±6 mm, ±8 mm and full acceptance windows for the right and left kidneys of the 10 volunteers. The r values increased with the size of acceptance windows, from a mean of approximately 50% at the acceptance window of ±4 mm to 100% at a full acceptance window. The full acceptance window with the gating-only algorithm is identical to an ungated scan. The a values also varied slightly with acceptance windows. However, a values varied widely among volunteers (SDs of approximately 0.12). The mean a values for both the right and left kidneys of the 10 volunteers were 0.61, 0.63, 0.63, and 0.66 for ±4, ±6, ±8 mm, and full acceptance windows, respectively.

A preset single a value is usually used for navigator scans. Because kidney motions can vary for different volunteers, δ could vary for different windows and volunteers. Table 3 lists the mean residual values of gating-and-following (δ) and gating-only (δ_0) algorithms as well as the improvement factor (δ_0/δ) calculated for different windows by using the mean a values given above for all the volunteers. The residual errors increase with the acceptance window for both gating-only and gating-and-following, because accepted diaphragm positions vary more greatly for a larger acceptance window. The mean δ values for all volunteers by the gating-and-following method ranged from 0.55 mm (±4 mm acceptance window) to 0.90 mm (full acceptance window) and those for the gating-only method ranged from 1.17 mm to 3.79 mm. When the gating-and-following method is adapted, the residual errors could be reduced by 123% – 890%, depending on different subjects and acceptance

windows. For a typical acceptance window of ±4 mm, improvements of 123% – 347% could be achieved. The residual errors increase with the acceptance widows due to the inclusion of larger displacements of diaphragm positions. However, this increase of the errors with the acceptance windows was significantly diminished by the introduction of the gating-and-following technique, because the large variations were corrected.

DISCUSSION

Although structural imaging of the kidneys can be completed within a breath-hold, functional imaging can last several minutes. For instance, it usually takes approximately 5 min to complete an arterial spin labeling (ASL) perfusion measurement. It is preferred that gating or other motion correction methods be used while performing such measurements. In addition, although healthy subjects may be able to tolerate multiple breath-held scans, the same may not be true for those who cannot hold their breath for prolonged periods, including young children. The navigator gating technique has been widely used to diminish motion artifacts and improve patient tolerance in MRI scans. Navigator gating is a standard technique on modern MRI scanners of most major vendors, and therefore available in many clinical MRI centers. Gating-and-following is performed by real-time processing, and no post-processing is required. The application is therefore transparent to the user and well suited for clinical practice. A preliminary study comparing image qualities showed that gating and following is more effective than gating only in correcting motion artifacts (8), but no quantitative comparison has been made to date between the two algorithms.

In this study, we found that the gating-and-following algorithm was more effective than the gating-only algorithm in reducing motion errors, as shown by a substantial reduction in the residual errors. The mean tracking factors obtained for different acceptance windows can be used to translate liver motion to kidney motion, which can help improve image quality and reduce scan time in navigator-gated MRI scans. The mean tracking factors provide a guideline for using the gating-and-following algorithm in navigator-gated scans.

Diaphragm/liver and kidney motion has been previously evaluated by different techniques. Wade measured diaphragm motion by fluoroscopy in 10 participants and found that the diaphragm moved 17 ± 3 mm in the SI direction (9). In a study of the diaphragm position by MRI in 15 volunteers (10), the mean maximum displacement of the diaphragm in the SI direction was 13 mm during normal breathing. In an ultrasound imaging study measuring kidney movement (11), the mean kidney movement in the SI direction was 11 ± 4 mm. Kidney motions in deep respiration were studied using fast MRI in fourteen patients, and found to be reproducible with a maximal displacement of 4.3 cm (14). In another study, the mean kidney motion measured by using CT images in 9 participants was 18 mm (12). The maximum displacements of the diaphragm and kidneys calculated from our study are in a good agreement with those reported in these studies.

The residual error of the gating-and-following algorithm is always lower than that of the gating-only algorithm as shown in Table 3, implying that the former is more effective in reducing motion errors. For gating-only, the residual errors increase with increasing size of the acceptance window, and the error could be up to 7.05 mm. Therefore, a narrow

acceptance window has to be used to achieve satisfactory image quality. When kidney displacements were followed using tracking factors, residual errors were found to be significantly reduced when the gating-and-following algorithm was used. The maximum residual error is decreased from 7.05 mm to 1.83 mm.

Acceptance rates increase as the size of the acceptance window increases as shown in Table 2, because more positions can be included in a larger acceptance window. However, the residual errors also increase with the acceptance window as shown in Table 3 because larger displacements of the accepted diaphragm positions are accepted for larger acceptance windows. The increase of residual errors with acceptance windows was reduced by up to 890% by applying the gating-and-following technique. Although a larger acceptance window is preferred for rapid scans, this can lead to a higher uncorrected motion error, resulting in poor image quality. Therefore, in a navigator-gated scan, the size of the acceptance window should be selected such that it reduces scan time without compromising on image quality.

Tracking factors can vary slightly between the left and right kidneys because of their different anatomic locations. However, generally a single mean tracking factor is used for both kidneys, suggesting that motion cannot be completely compensated in a navigator-gated scan. Nevertheless, in our study, the difference in tracking factors for the 2 kidneys was less than 0.10 for most volunteers, which is likely acceptable for most MRI scans. Since gating-and-following in navigator gated scans only compensates the organ shift movements, other forms of motions such as rotation and deformation were not investigated in this study.

Our study shows that kidneys can move away from the desired imaging position by an average of approximate 3.7 mm without gating, which can severely degrade image quality. Navigator gating can substantially reduce this motion error – mean improvements of 166% can be achieved for an acceptance window of 4 mm by the gating-only method and of 329% for the same acceptance window by the gating-and-following method. This improvement is even higher for large acceptance windows for the gating-and-following method. On the other hand, this improvement can be traded for a larger acceptance window to reduce scan time. If the error (1.06 mm) of the gating-only method can be tolerated with a 4 mm acceptance window, the window can even be increased to a full acceptance window, in which the mean motion error of 0.90 is still lower than that obtained by using the gating-only method with an acceptance window of 4 mm. However, with the full acceptance window, the scan time could be reduced by approximately 50%.

This study and the gating-and-following method have limitations. Normal respiration is assumed when using tracking factors in gating-and-following. The results of this study may not be applicable to patients with respiratory disorders. The age range of the volunteers is limited to 21 to 46 years. Tracking factors of other populations, e.g. children, may be different than found here. Adapted studies may be needed to identify optimum tracking factors in these specific patient groups. In applications where continuous image collection is needed and timing is critical, e.g. dynamic contrast enhanced MRI, navigator gating cannot be used since a certain percentage of images will be rejected.

In conclusion, the relationship between the liver and kidney movements were systematically analyzed and tracking factors were obtained in healthy volunteers. Our study suggests that gating-and-following is superior to gating-only for navigator scans. Based on the presented results, tracking factors can be chosen for navigator supported renal imaging, and the width of the acceptance window can be optimized depending on the required image quality and preferred scan time.

Acknowledgments

Grant supports:

NHLBI 5 U54HL070590-06 (Scholar) and the American Lebanese Syrian Associated Charities (ASLAC)

We thank Dr. Vani J. Shanker at the Department of Scientific Editing, St. Jude Children's Research Hospital for scientific editing.

References

1. Huang AJ, Lee VS, Rusinek H. Functional renal MR imaging. Magn Reson Imaging Clin N Am. 2004; 12(3):469–486. [PubMed: 15271366]
2. Katzberg RW, Buonocore MH, Low R, Hu B, Jain K, Castillo M, Troxel S, Nguyen MM. MR determination of glomerular filtration rate in subjects with solitary kidneys in comparison to clinical standards of renal function: feasibility and preliminary report. Contrast Media & Molecular Imaging. 2009; 4(2):51–65. [PubMed: 19274681]
3. Martirosian P, Klose U, Mader I, Schick F. FAIR true-FISP perfusion imaging of the kidneys. Magnetic Resonance in Medicine. 2004; 51(2):353–361. [PubMed: 14755661]
4. Song R, Loeffler RB, Hillenbrand CM. Improved renal perfusion measurement with a dual navigator-gated Q2TIPS fair technique. Magn Reson Med. 2010; 64:1352–1359. [PubMed: 20593428]
5. Thoeny HC, De Keyzer F, Oyen RH, Peeters RR. Diffusion-weighted MR imaging of kidneys in healthy volunteers and patients with parenchymal diseases: initial experience. Radiology. 2005; 235(3):911–917. [PubMed: 15845792]
6. Prasad PV, Edelman RR, Epstein FH. Noninvasive evaluation of intrarenal oxygenation with BOLD MRI. Circulation. 1996; 94(12):3271–3275. [PubMed: 8989140]
7. Ehman RL, Felmlee JP. Adaptive technique for high-definition MR imaging of moving structures. Radiology. 1989; 173(1):255–263. [PubMed: 2781017]
8. Danias PG, McConnell MV, Khasgiwala VC, Chuang ML, Edelman RR, Manning WJ. Prospective navigator correction of image position for coronary MR angiography. Radiology. 1997; 203(3): 733–736. [PubMed: 9169696]
9. Wade OL. Movements of the thoracic cage and diaphragm in respiration. J Physiol. 1954; 124(2): 193–212. [PubMed: 13175123]
10. Korin HW, Ehman RL, Riederer SJ, Felmlee JP, Grimm RC. Respiratory kinematics of the upper abdominal organs: a quantitative study. Magn Reson Med. 1992; 23(1):172–178. [PubMed: 1531152]
11. Davies SC, Hill AL, Holmes RB, Halliwell M, Jackson PC. Ultrasound quantitation of respiratory organ motion in the upper abdomen. Br J Radiol. 1994; 67(803):1096–1102. [PubMed: 7820402]
12. Balter JM, Haken RKT, Lawrence TS, Lam KL, Robertson JM. Uncertainties in CT-based radiation therapy treatment planning associated with patient breathing. Int J Radiat Oncol Biol Phys. 1996; 36(1):167–174. [PubMed: 8823272]
13. Oppelt A, Gaumann R, Barfuss H, Fischer H, Hartl W, Schajor W. FISP: eine neue schnelle Pulssequenz für die Kernspintomographie. Electromedica. 1986; 54:15–18.
14. Schwartz LH, Richaud J, Buffat L, Touboul E, Schlienger M. Kidney mobility during respiration. Radiotherapy and Oncology. 1994; 32(1):84–86. [PubMed: 7938682]

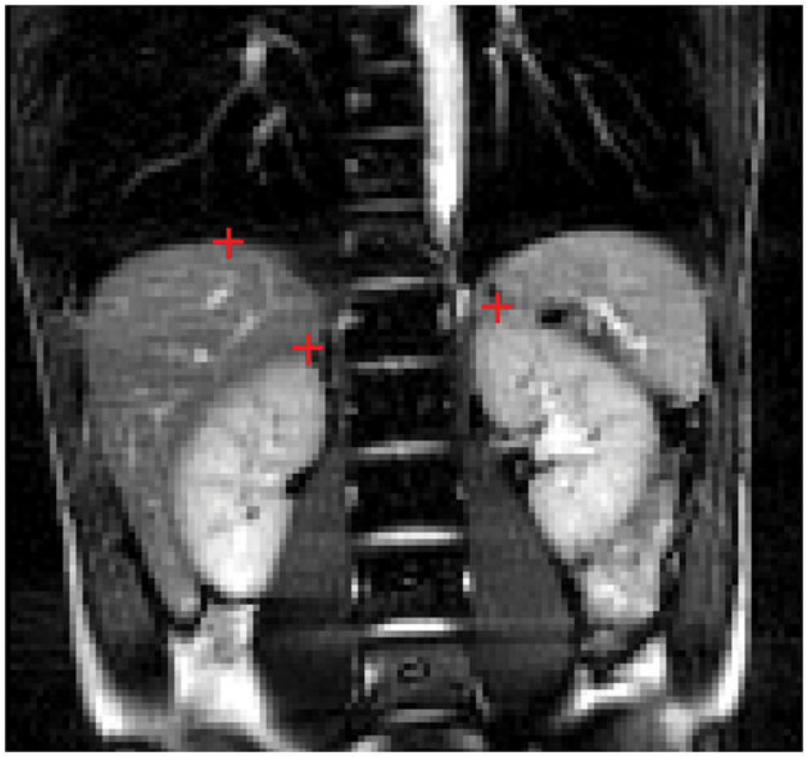

FIG. 1.

One typical coronal image obtained with True-FISP out of 200 images. Red crosses are the representative points of the kidney and liver, which were chosen at the top of liver dome and the superior pole of the kidney, respectively.

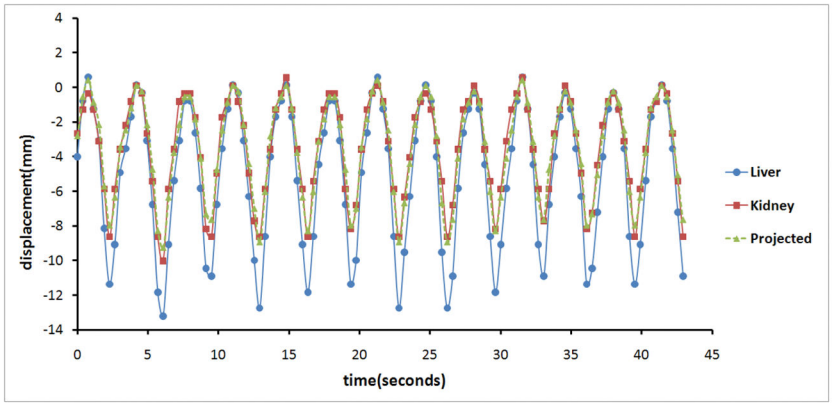

FIG. 2.

Movement patterns of the liver (blue line with solid circles) and kidney (red line with solid squares) along with the projected displacement (green line with solid diamonds) of the kidney based on the liver motion. The projected kidney motion is in a good agreement with the true kidney motion. The respective marks represent the measured or calculated positions.

Table 1

Maximum displacements of the liver and kidneys of the 10 healthy volunteers, along with heights and weights

volunteer			maximum displacement(mm)		
	weight(kg)	height(cm)	liver	right kidney	left kidney
1	56	167	8.6±3.1	5.1± 0.9	6.6±1.3
2	55	167	15.5±2.4	6.5±1.1	8.7±0.8
3	63	162	12.8±2.0	9.2±1.5	10.6±1.2
4	56	167	14.2±2.7	12.8±1.5	6.2 ±2.8
5	70	170	10.1±4.2	7.3±3.0	6.6±3.1
6	80	182	16.8±5.4	15.1±4.4	13.9±7.0
7	80	172	7.8±2.4	6.7±0.67	4.8±0.8
8	79	190	7.8±2.8	4.4±1.6	5.6± 0.7
9	84	180	22.5±2.3	13.8±1.7	12.3±2.1
10	83	188	11.8±1.0	8.5±0.5	9.5±0.9
Mean±SD	70.6±12	170±10	12.8±4.6	8.9±3.7	8.48±3.04

Table 2

Acceptance rates (r) and tracking factors (a) for various acceptance windows for the ten volunteers.

V	window (mm)	right kidney				left kidney			
		4	6	8	full	4	6	8	full
1	r	61%	75%	93%	100%	56%	69%	82%	100%
	a	0.54	0.59	0.61	0.63	0.57	0.55	0.59	0.62
2	r	54%	60%	69%	100%	35%	51%	55%	100%
	a	0.43	0.44	0.47	0.47	0.4	0.45	0.46	0.47
3	r	34%	47%	57%	100%	48%	57%	68%	100%
	a	0.63	0.64	0.68	0.76	0.72	0.76	0.79	0.75
4	r	48%	55%	59%	100%	59%	71%	84%	100%
	a	0.55	0.58	0.53	0.7	0.55	0.57	0.56	0.61
5	r	54%	71%	87%	100%	48%	64%	76%	100%
	a	0.68	0.69	0.71	0.71	0.58	0.53	0.55	0.55
6	r	60%	65%	70%	100%	36%	45%	55%	100%
	a	0.73	0.8	0.84	0.92	0.74	0.8	0.78	0.84
7	r	50%	73%	100%	100%	59%	79%	93%	100%
	a	0.76	0.76	0.78	0.78	0.65	0.62	0.61	0.6
8	r	81%	95%	97%	100%	45%	62%	82%	100%
	a	0.74	0.75	0.75	0.74	0.62	0.54	0.53	0.53
9	r	27%	34%	43%	100%	27%	34%	43%	100%
	a	0.58	0.57	0.54	0.6	0.56	0.56	0.56	0.53
10	r	54%	63%	71%	100%	48%	56%	67%	100%
	a	0.68	0.68	0.71	0.7	0.53	0.61	0.63	0.66
mean ±SD	r	52±15%	64±17%	75±19%	100%	46±11%	59±13%	71±16%	100%
	a	0.63±.10	0.65±.11	0.66±.12	0.70±.12	0.59±.10	0.60±.11	0.61±.11	0.62±.11

V: Volunteer.

Table 3

Mean residual errors of gating-and-following (δ) and gating-only (δ_0) algorithms and the improvement factor (δ/δ_0) for different acceptance windows (mm) in the ten volunteers*.

V	window (mm)	right kidney				left kidney			
		4	6	8	full	4	6	8	full
1	δ(mm)	0.43	0.44	0.45	0.48	0.88	0.89	0.9	0.91
	δ_0(mm)	0.85	1.21	1.79	2.11	1.15	1.45	1.94	2.79
	δ_0/δ	*198%*	*274%*	*397%*	*442%*	*131%*	*162%*	*216%*	*307%*
2	δ(mm)	0.42	0.48	0.55	1.2	0.61	0.75	0.77	1.6
	δ_0(mm)	0.73	0.87	1.21	2.63	0.76	1.25	1.41	3.63
	δ_0/δ	*172%*	*180%*	*218%*	*220%*	*123%*	*166%*	*182%*	*228%*
3	δ(mm)	0.54	0.58	0.63	0.9	0.54	0.57	0.68	0.75
	δ_0(mm)	1.29	1.78	2.34	4.9	1.02	1.44	2.15	4.37
	δ_0/δ	*238%*	*308%*	*373%*	*543%*	*189%*	*254%*	*315%*	*582%*
4	δ(mm)	0.55	0.57	0.62	0.81	0.78	0.76	0.88	0.86
	δ_0(mm)	1.05	1.32	1.46	4.77	1.16	1.42	1.77	2.55
	δ_0/δ	*192%*	*232%*	*236%*	*590%*	*149%*	*185%*	*202%*	*294%*
5	δ(mm)	0.38	0.41	0.48	0.5	0.79	0.76	0.76	0.97
	δ_0(mm)	1.3	1.83	2.43	3.02	1.24	1.57	1.95	2.99
	δ_0/δ	*347%*	*444%*	*505%*	*604%*	*158%*	*207%*	*258%*	*309%*
6	δ(mm)	0.88	0.92	1	1.83	0.45	0.57	0.65	1.53
	δ_0(mm)	1.3	1.57	1.9	5.41	1.21	1.75	2.42	7.05
	δ_0/δ	*148%*	*171%*	*191%*	*297%*	*269%*	*305%*	*374%*	*460%*
7	δ(mm)	0.55	0.62	0.78	0.69	0.35	0.34	0.36	0.4
	δ_0(mm)	1.34	2.18	3.19	3.19	0.92	1.42	1.84	2.05
	δ_0/δ	*244%*	*348%*	*406%*	*459%*	*266%*	*413%*	*505%*	*510%*
8	δ(mm)	0.78	0.79	0.81	0.78	0.54	0.64	0.74	0.87
	δ_0(mm)	1.26	1.65	1.71	1.86	1.1	1.5	2.03	2.64
	δ_0/δ	*161%*	*208%*	*212%*	*238%*	*204%*	*234%*	*275%*	*302%*
9	δ(mm)	0.63	0.62	0.68	0.88	0.42	0.43	0.62	0.66